

# Evidence that cuprate superconductors form an array of nanoscopic Josephson junctions

Hércules S. Santana and E. V. L. de Mello<sup>1</sup>

<sup>1</sup>*Instituto de Física, Universidade Federal Fluminense, 24210-346 Niterói, RJ, Brazil\**

Recent measurements of charge instabilities in overdoped compounds rekindled the proposal that cuprates become superconductors by long-range order through Josephson coupling between nanoscopic charge domains. We use the theory of phase-ordering dynamics to show that incommensurate charge density waves (CDWs) are formed in the CuO planes by a series of free-energy wells separated by steep barriers. Charge oscillations in these domains give rise to a net hole-hole attraction proportional to the height of these barriers. Concomitantly, the self-consistent calculations yield localized superconducting amplitudes in the CDW domains characterizing a granular superconductor. We show that a transition by long-range phase order promoted by Josephson coupling elucidates many well-known features of cuprates like the high magnetic penetration depth anisotropy and the origin of the pseudogap, among others. Furthermore, the average Josephson energy reproduces closely the planar superfluid density temperature dependence of La-based films and the superconducting giant proximity effects of cuprates, a 20-year-old open problem.

## I. INTRODUCTION

One of the main challenges of condensed-matter physics is a complete theory for high critical temperature superconductors (HTSs). Such a theory has been hindered by many issues like the absence of clear Fermi surfaces, the pseudogap, and the prominence of various forms of collective fluctuations<sup>1</sup>. To characterize whether these distinct orders compete with or strengthen each other, many experimental techniques have been refined to detect even overlapping fluctuations. After imaging a granular structure with high spatial resolution scanning tunneling microscopy (STM) in underdoped  $\text{Bi}_2\text{Sr}_2\text{CaCu}_2\text{O}_{8+d}$  (Bi2212), Lang *et al*<sup>2</sup> proposed that superconducting (SC) long-range order could be achieved by Josephson coupling between nanoscopic domains. This idea gained more recognition after the measurements of CDW in  $\text{YBa}_2\text{Cu}_3\text{O}_{6+x}$  (YBCO) single crystals but was still not considered as a general theory of cuprates for two reasons: first, the absence of incommensurate charge ordering (CO) or CDW data in the overdoped region and, second, the lack of a theoretical model that could justify and describe the physical formation of the small Josephson junctions between the CO domains.

In this paper, we use the theory of phase-ordering dynamics to show that the CDW or CO may be formed by a two-dimensional array of free energy potential wells with similar properties of granular superconductors. In recent years there was a great improvement in the precision of the CO wavelength  $\lambda_{\text{CO}}$  measurements by STM, x-ray, and Resonant X-Ray Scattering (REXS)<sup>3</sup>. The very fine variation of  $\lambda_{\text{CO}}$  with the doping  $p$  (or hole per CuO unit cell) revealed in these experiments can be reproduced theoretically by a phase separation formalism based on the time-dependent nonlinear Cahn-Hilliard (CH) differential equation<sup>4</sup>. In this approach, the charge modulations may be tuned up to reproduce the measured  $\lambda_{\text{CO}}(p)$  on 100% volume fraction of the simulations<sup>5-9</sup>.

The phase separation free energy reproduces the CDW structure and acts as a crystal field that promotes the Cooper pair formation, leading to a direct connection between the SC interaction and the charge modulations. Some critique the CDW-mediated superconductivity, arguing that

CDW is limited to the underdoped region. However recent measurements<sup>10-12</sup> and new x-ray diffraction demonstrated CDW correlations in overdoped  $\text{La}_{2-x}\text{Sr}_x\text{CuO}_4$  (LSCO) up to compounds of at least  $x \equiv p = 0.21$  and possibly up to  $p = 0.25$ <sup>13</sup>. Here we perform CDW simulations and develop a SC theory of cuprates based on Josephson coupling between local SC order parameters in these domains and their long-range phase order (LRO). The Josephson coupling is closely related with the superfluid density<sup>14,15</sup>  $\rho_{\text{sf}}$  and reproduces its measured temperature variation  $\rho_{\text{sf}}(T)$  of several overdoped LSCO films with great accuracy.

The CDW-LRO approach is also appropriate to describe the giant proximity effects (GPE) experiments in YBCO S-I-S wires<sup>16</sup> and in LSCO Josephson type trilayers S-N'-S junctions<sup>17,18</sup> where I is an insulator with nonzero doping, S is a superconductor, and N' is a superconductor layer in the normal phase. According to conventional theory, the critical current should diminish exponentially with the size  $d$  of a barrier made of non-SC materials<sup>17</sup>. For traditional low temperature Josephson junctions the thickness of the barrier  $d$  is generally comparable with the barrier coherence length<sup>17</sup>  $\xi_{\text{N}}$ . However, despite the very small SC coherence lengths  $\xi_{\text{SC}}$  of cuprates, GPE was measured with several large barriers<sup>16,17</sup> with  $d \gg \xi_{\text{N}}$ . Thus, technically the YBCO non-SC spacer with  $d \sim 100$  nm and La-based trilayers with  $d \sim 100 - 1000$  nm are too large to carry a critical current, in clear contradiction with the experiments<sup>16-18</sup>. On the other hand, in our approach, S, N', and I all have CDW and differ only by the presence or absence of LRO, which is very sensitive to external perturbations like an applied current or magnetic field.

## II. THE CDW SIMULATIONS

The starting point is the definition of the time-dependent phase separation (PS) order parameter associated with the local electronic density,  $u(\mathbf{r}, t) = [p(\mathbf{r}, t) - p]/p$ , where  $p$  is the average hole density and  $p(\mathbf{r}, t)$  is the charge density at a position  $\mathbf{r}$  in the CuO plane and at a time of simulation  $t$ . The CH equation is based on the electronic phase separation Ginzburg-Landau (GL) free energy expansion in terms of the

conserved charge order parameter  $u^{5-9,19}$ .

$$f(u) = \frac{1}{2}\varepsilon|\nabla u|^2 + V_{\text{GL}}(u, T), \quad (1)$$

where  $\varepsilon$  is the parameter that controls the charge modulations scale and  $V_{\text{GL}}(u, T) = -\alpha[T_{\text{PS}} - T]u^2/2 + B^2u^4/4 + \dots$  is a temperature-dependent double-well potential that characterizes the rise of charge oscillations below the onset of phase separation temperature  $T_{\text{PS}}$ . We do not know  $T_{\text{PS}}$ , but there are indications that it is close to the pseudogap temperature  $T^*$ . In the simulations, when  $T \leq T^*$ , the values of  $\alpha$  and  $B$  are always one. This free energy in terms of the phase separation order parameter is much simpler than the Ginzburg-Landau-Wilson free energy in terms of SC and pair density wave fields (PDW)<sup>20</sup>, but it suitably reproduces the details of the CO structure of distinct compounds and their localization energy  $V_{\text{GL}}$ .

The CH equation can be written derived by a continuity equation of the local free energy current density  $\mathbf{J} = M\nabla(\delta f/\delta u)$ ,<sup>23</sup>

$$\begin{aligned} \frac{\partial u}{\partial t} &= -\nabla \cdot \mathbf{J} \\ &= -M\nabla^2[\varepsilon^2\nabla^2 u - \alpha^2(T)u + B^2u^3], \end{aligned} \quad (2)$$

where  $M$  is the mobility or the charge transport coefficient that sets both the phase separation time scale and the contrast between the values of  $u$  for the two phases.

The equation is solved by a stable and fast finite difference scheme with free boundary conditions<sup>19</sup>, yielding the phase separation order parameter  $u(\mathbf{r}, t = n\delta t)$ , function of position  $\mathbf{r}$  and  $n$  simulation time step  $\delta t$ . The limiting cases are  $u(\mathbf{r}_i, t) \approx 0$ , corresponding to homogeneous systems above or near  $T_{\text{PS}}$  or small charge variations like the observed CDW, and  $u(\mathbf{r}_i, t \rightarrow \infty) = \pm 1$ , corresponding to the extreme case (at low temperatures) of complete phase separation. The local charge density is derived from  $p(\mathbf{r}, t) = p \times (u(\mathbf{r}, t) + 1)$ , and the latter case (strong phase separation) applies to static stripes<sup>24,25</sup>, while the former (weak phase separation) to very small  $\Delta p \approx 10^{-2-3}$  variations around  $p$ , like that measured in  $\text{YBa}_2\text{Cu}_3\text{O}_{6+\delta}$  (Y123)<sup>26</sup>.

Figure 1(a) shows that below the  $T_{\text{PS}}$  temperature the order parameter  $u(\mathbf{r}, t)$  evolves in time and  $V_{\text{GL}}(\mathbf{r}, t)$  valleys become deeper, which is expected to occur when the temperature decreases, favoring the mesoscopic phase separation. As the temperature goes below  $T^*$ , we assume the large time behavior  $V_{\text{GL}}(\mathbf{r}, t \rightarrow \infty)$  shown in Fig. 1(a) to become the low temperature  $V_{\text{GL}}(\mathbf{r}, T \rightarrow 0)$  that generates the CDW [Fig. 1(b)]. In this large time regime,  $V_{\text{GL}}(\mathbf{r})$  depends on the temperature through the usual form of the first GL coefficient defined after Eq. 1, that is,  $(1 - T/T^*)^2$ . This temperature dependence is the only relevant dependence of  $V_{\text{GL}}(\mathbf{r}, T)$  in our calculations.

A typical later time and low-temperature  $V_{\text{GL}}(u(\mathbf{r}))$  used in the calculations is shown in Fig. 2(b), which leads to the LSCO checkerboard structure. We also show the three-dimensional side view (in the inset) with its wells or valleys in form of ‘‘ice cream cones’’. Notice that the free energy is

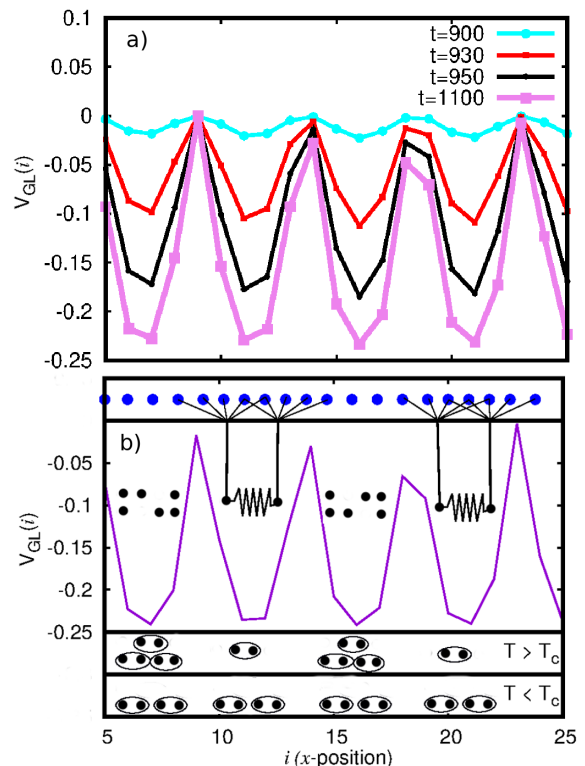


FIG. 1. (a) The  $V_{\text{GL}}(t)$  evolution with time. Initially,  $V_{\text{GL}}$  is flat, which corresponds to a system above the onset phase separation temperature  $T_{\text{PS}}$ . The phase separation potential wells or valleys increase with time, and this behavior is correlated with the decrease of the temperature below  $T_{\text{PS}}$ . As the temperature goes below  $T^*$ , we assume the stable large time behavior  $V_{\text{GL}}(t \rightarrow \infty)$  to be that of low temperature  $V_{\text{GL}}(T \leq T^*)$ . (b) The Cooper pair formation in the CDW free energy valleys. At the top, we represent some planar Cu atoms (blue-filled circles) attracted to hole-poor domains represented by black lines as an illustration. Hole fluctuations in these domains produces atomic fluctuations that affect also the other holes, promoting an atomic mediated interaction (represented by the springs as an illustration). At low temperature ( $T \leq T^*$ ) the Cooper pairs may be formed in the CDW valleys (the encircled pair of black dots), and at  $T \leq T_c$  they superflow and become uniform on the CuO plane (in agreement with the CO x-ray scattering decreasing signal below  $T_c$ <sup>21,22</sup>).

defined over the CuO plane, and the third dimension is its values in each site, which demonstrates that the minima occur at the center of the charge domains and the maxima at the borders. The detailed structure and strength of this potential is shown in the Supplemental Material<sup>27</sup>.

For YBCO, the CDW domains are formed in puddles or patches with different modulation in either  $a$  or  $b$ -direction in the CuO plane<sup>28,29</sup>. The LRO superconducting calculations with  $V_{\text{GL}}(u(\mathbf{r}))$  and alternating stripe-like puddles follow in the same way of the checkerboard of Fig. 2 since the method requires only the formation of such finite-charge domains<sup>9</sup>. We emphasize that the calculations described and performed here are pure two dimensional in order to model the observed charge arrangements on the CuO plane and does not take into

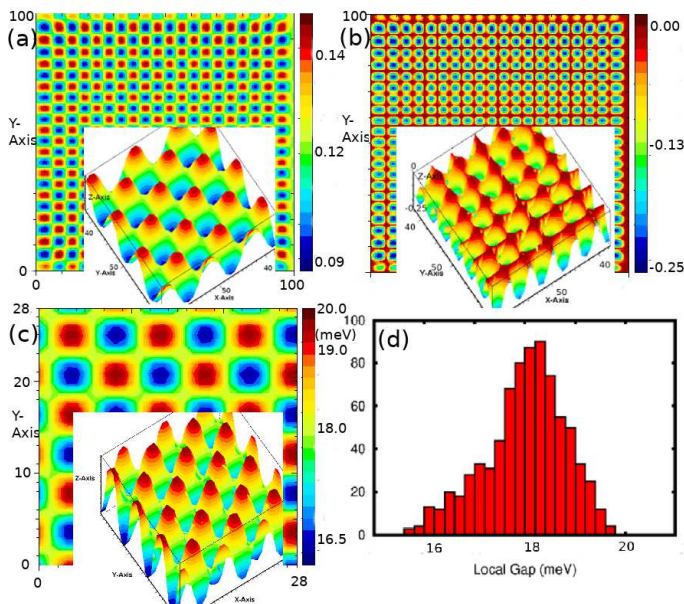


FIG. 2. Top and three dimensional perspective of different properties at a later time or low temperature: (a) A checkerboard CDW map for a LSCO system with average hole density  $p = 0.12$  on a  $100 \times 100$  unit cell simulations and out of plane view. (b) The corresponding GL free energy potential  $V_{GL}(\mathbf{r}_i)$ . The inset shows the three-dimensional perspective, which reveals the array of deep wells. (c) The BdG SC amplitude  $\Delta_d(\mathbf{r}_i)$  map in a  $28 \times 28$  unit cell portion of the density map of (a). The three-dimensional perspective plot demonstrates that the amplitudes  $\Delta_d(\mathbf{r}_i)$  are completely localized inside the CDW domains. (d) Typical histogram of the amplitudes  $\Delta_d(\mathbf{r}_i)$  variation with the local  $p_i$  concentration.

account possible out-of-plane influences, like the quenched disorder which arises from oxygen interstitials discovered in the in  $\text{HgBa}_2\text{CuO}_{4+y}$  system<sup>30</sup>.

### III. SUPERCONDUCTING CALCULATIONS

The new form of analysis here is the three-dimensional view of the planar CDW maps shown in Fig. 2(a), the GL free energy potential  $V_{GL}$  in Fig. 2(b), and the SC pair amplitude  $\Delta_d(\mathbf{r}_i)$  in a  $28 \times 28$  site portion of the  $100 \times 100$  site density map from Fig 2(a) in Fig. 2(c). These illustrative plots are for an LSCO sample with an average hole density  $p = 0.12$ . These plots show clearly that alternating rich and poor charge regions develop in the same kind of valleys in the form of “ice cream cones”, as it is demonstrated by the out-of-plane view of the insets. The SC pair amplitudes inside the wells in Fig. 2(c) have the same properties of isolated SC grains, which motivates the proposal of an array of Josephson junctions.

While Fig. 1(a) shows the evolution of  $V_{GL}(x_i)$  that leads to the CDW, Fig. 1(b) shows the low-temperature  $V_{GL}(x_i)$  that leads to the formation of the SC interaction in the CuO planes. At the top we represent some planar atoms (blue circles) attracted (repelled) by hole-poor (hole-rich) CDW domains represented schematically by black lines. High-energy

x-ray diffraction<sup>22</sup> revealed that CDW modulations displace the Cu and O atoms whose oscillations around their equilibrium positions are sensed by the holes and may give rise to a net hole-hole attraction<sup>9,15</sup> illustrated by the springs.

We argued before that this induced hole-hole SC interaction is proportional to the depth of the  $V_{GL}$  wells averaging over the whole system, that is,  $\langle V_{GL}(p) \rangle$ <sup>9,15</sup>. The mean-field self-consistent Bogoliubov-de Gennes (BdG) calculations with this attractive pair interaction over the whole system yield the local pair amplitude map  $\Delta_d(\mathbf{r}_i)$ . The results also depend on the local hole density  $p(i)$  and, consequently, have the same CDW modulations ( $\lambda_{CO}$ ), leading to what is known as pair density wave<sup>1</sup>.

Since the  $\Delta_d(\mathbf{r}_i)$  fit perfectly inside the wells, each CDW domain has an independent local SC order parameter phase  $\phi_i$ , exactly as a granular superconductor. Therefore, each CDW domain may behave like mesoscopic SC grains interconnected by Josephson junctions with energies  $E_J(\mathbf{r}_{lm})$  between  $l$  and  $m$  domains like those shown with alternate red and blue colors in Fig. 2(c). In the bottom of Fig. 1(b) we show that, according to previous calculations<sup>9,15</sup>, the Cooper pairs are present up to  $T \leq T^*$  and are represented by two encircled black dots. At  $T \leq T_c$ , LRO sets in, and the Cooper pairs superflow through the system, establishing a uniform charge density on the CuO plane. This leads to a decrease of the CDW signal observed by high-energy x-ray diffraction below  $T_c$ <sup>21,22</sup> and was widely interpreted by due to the competition between CDW and superconductivity. We emphasize that our calculations establish the opposite: The CDW hosts the charge domains and the local Cooper pairs in alternating domains, but they spread through the system when LRO sets in at  $T \leq T_c$ . This is shown schematically at the bottom of Fig. 1(b).

Following the above arguments,  $T_c$  is determined by the competition between thermal disorder and the average planar Josephson energy  $\langle E_J(p, T) \rangle$  that depends also on the spatial averaged  $d$ -wave pair amplitude

$$\langle \Delta_d(p, T) \rangle = \sum_i^N \Delta_d(\mathbf{r}_i, p, T) / N, \quad (3)$$

where the sum, like in the case of  $\langle V_{GL}(p) \rangle$ , is over the  $N$  unit cells of a CuO plane. As explained previously<sup>8,9</sup>, the  $d$ -wave relation for the average Josephson coupling energy is proportional to the  $s$ -wave expression<sup>31</sup>:

$$\langle E_J(p, T) \rangle = \frac{\pi \hbar \langle \Delta_d(p, T) \rangle}{4e^2 R_n(p)} \tanh \left[ \frac{\langle \Delta_d(p, T) \rangle}{2k_B T} \right]. \quad (4)$$

Here  $R_n(p)$  is the average planar tunneling resistance between the grains that is assumed to be proportional to the in-plane normal state resistance just above  $T_c$ . In the array of Josephson junction model, the current is composed of Cooper pairs tunneling between the CDW domains and by the normal carriers or quasi-particle plane current<sup>32</sup>. For a  $d$ -wave HTS near  $T_c$  the supercurrent is dominant<sup>32</sup>, which justifies the use of the experimental  $R_n(p)$  in the above equation. Therefore, LRO is attained when the average  $\langle E_J(p, T) \rangle$  is strong enough



to overcome thermal phase disorder, or  $\langle E_J(p, T_c) \rangle = k_B T_c$ , and that is how we derive  $T_c$ <sup>8,9,33,34</sup>.

These in-plane calculations are the basic pillars to the three-dimensional LRO in the whole system, which we may infer from transport measurements. For low  $p$ , just above  $T_c$ , the  $z$ -direction resistivity  $\rho_c$  is  $\approx 10^3 - 10^6$  larger than the  $a$  or  $b$ -axis resistivity<sup>35,36</sup>. Despite this large difference, it is surprising that both  $\rho_c(T)$ , and  $\rho_{ab}(T)$  fall to zero at the same temperature ( $T_c$ ) and this puzzling behavior can be understood in terms of the Josephson coupling of Eq. 4. The smaller planar resistances yield larger  $E_J$  that promote first LRO in the planes, but each plane  $i$  would have its own SC phase  $\theta_i$  if it was not for the weaker inter-plane  $E_J$  coupling. Thus the  $z$ -direction Josephson coupling connects the planes, leading to only a single-phase  $\theta$  in the whole system, and both  $z$  and  $ab$  resistivity drop off together at  $T_c$ , which is a plausible explanation for this long-known non-conventional result. Again using Eq. 4, a smaller low temperature superfluid density is expected along the  $z$ -direction than along the plane, which is confirmed by the measured large anisotropy of  $ab$  and  $c$ -axis magnetic penetration depth<sup>37,38</sup>. Thus, although  $z$ -direction coupling is fundamental, the SC properties like the local SC amplitudes  $\Delta_d(\mathbf{r}_i, p, T)$  and  $T_c(p)$  develop and depend entirely on the CuO planes.

#### IV. THE SUPERFLUID DENSITY

For low-temperature superconductors, the temperature  $T_\theta$  at which LRO disappears is very large compared with  $T_c$ , but they are estimated to be comparable for HTS<sup>39</sup>. Our basic point is that  $T_c = T_\theta$ , and at higher temperatures, the Cooper pairs in the nanoscopic grains have all different  $\theta_i$  and, consequently are in an incoherent state. This approach leads us to infer a close connection between Josephson coupling and superfluid phase stiffness.

The first thing to notice is that  $J_c(T)$  is proportional to the two-dimensional (2D) superfluid density  $n_s(T)$  or the local Josephson current<sup>14</sup> that is also proportional to the phase stiffness  $\rho_{sc}$ <sup>40</sup>. Along these lines, we made  $\langle E_J(p, 0) \rangle$  equal to the 2D zero-temperature superfluid phase stiffness<sup>15,33</sup>  $\rho_{sc}(p, 0)$  and reproduced the measured scale relation between the zero temperature superfluid density and  $T_c(p)$ . To underdoped compounds, this relation is known as Uemura's law<sup>41</sup>, and a similar relation for La-based overdoped films was obtained more recently<sup>40</sup>.

Along these lines, we show in Fig. 3 that  $(\langle E_J(p, T) \rangle / k_B - T)$  reproduces the measured<sup>40</sup> 2D phase stiffness  $\rho_{sc}(p, T)$  temperature dependence. The plots show very good agreement with  $p = 0.16$  and  $0.19$  films according to Ref. [40]. For  $p = 0.22$  we could extract with certainty only the experimental values at  $T = 0$  and  $T_c$ , but the theory seems to reproduce closely also the intermediate data. In the plots we used  $\langle E_J(p, T) \rangle$  from Eq. 4 with  $\langle \Delta_d(p, T) \rangle$  and  $R_n(p)$  derived previously in Refs.[15,33].

Another indication that  $\langle E_J(p, 0) \rangle / k_B - T$  is equal to  $\rho_{sc}(p, T)$  comes from the proximity effect experiment on YBCO wires<sup>16</sup>. They measured the critical current  $I_c$  through

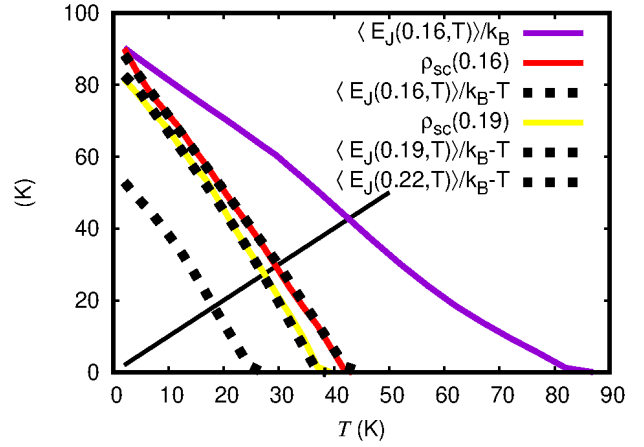


FIG. 3. Comparison between the measured phase stiffness  $\rho_{sc}(p, T)$  for La-based films with  $p = 0.16, 0.19$ , and  $0.22$  from Ref.[40] and  $(\langle E_J(p, T) \rangle / k_B - T)$  (dashed lines), with an almost perfect agreement. We show also the Josephson coupling  $\langle E_J(0.16, T) \rangle$  that sets the SC phase order scale  $T_\theta$  derived in Ref. [15] and the temperature  $T$  to make clear how to derive  $T_c(p = 0.16)$ .

a small insulator region of size  $d$  inserted in the SC wire. In their Fig. 2(b), they showed that the product  $I_c R_n$  at low-temperature is constant for several values of  $d$  from 40 to 110 nm, which is much larger than the estimated coherence length  $\xi_{SC}$  of 9 nm<sup>16</sup>. We interpret this result recalling that the low-temperature Josephson current is<sup>42</sup>

$$I_J = \frac{E_J(0)}{\hbar/(2e)} = \frac{\pi \Delta_d(0)}{2e R_n} \quad (5)$$

Following the above discussion, taking  $I_J = I_c \propto \langle E_J(p, 0) \rangle$  and according to Eq. 4, the product  $I_c R_n$  is independent of the insulator spacer  $d$ , in perfect agreement with the measurements with the S-I-S YBCO junctions. This result, in the framework of our theory, suggests that the CDW is also present in the underdoped insulator part of the YBCO wire, in agreement with the connection between CDW and the antinodal PG mentioned in the previous section<sup>43,44</sup>.

#### V. RESULTS AND DISCUSSION

In general, the critical current density is the product of the superfluid velocity and density, that is,  $J_c = v_s \rho_{sc}$ . We have shown above that  $\langle E_J(p, T) \rangle / k_B - T$  is equal to  $\rho_{sc}(T)$  and that the low-temperature critical current  $I_c(0) \propto \langle E_J(p, 0) \rangle$  on the YBCO wires<sup>16</sup>. Based on these two results, we assume that the average superfluid velocity is  $v_s \propto \langle E_J(p, T) \rangle / \langle E_J(p, 0) \rangle$  and that,

$$J_c(T) \propto (\langle E_J(p, T) \rangle / k_B - T) \frac{\langle E_J(p, T) \rangle}{\langle E_J(p, 0) \rangle}. \quad (6)$$

This expression will be used to compare with the GPE measured critical currents<sup>16,17</sup>.

The first system to deal here is the trilayers along the  $z$  direction composed of  $\text{La}_{1.85}\text{Sr}_{0.15}\text{CuO}_4$  films with  $T_c \approx 45$  K (S) and the underdoped superconductor  $\text{La}_2\text{CuO}_{4+\delta}$  with  $T'_c \approx 25$  K (N') sandwiched according to Ref.[17]. Initially we study S and N' separately, with the average amplitudes  $\langle \Delta_d(p = 0.12, T) \rangle$  and  $\langle \Delta_d(p = 0.15, T) \rangle$ <sup>15,33</sup> and the factor of three in their normal resistances  $R_n$  just above their  $T_c$  according to Ref. [45]. For  $T \leq 25$  K there is LRO in both S and N'. Therefore, in principle,  $J_c$  would be limited by the lower  $T'_c \approx 25$  K, but they measured a persisting  $J_c$  almost to  $T = 35$  K independently of the number of underdoped N' layers<sup>17</sup>.

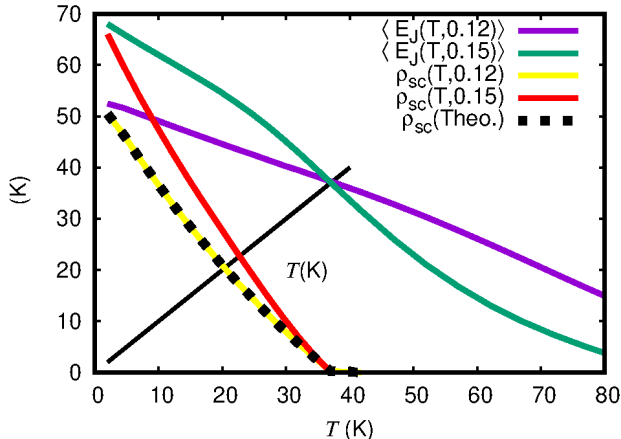


FIG. 4. S and N' layers plots after they are connected in the S-N'-S structure both with the average hole density  $p' = 0.135$ .  $\langle E_J(p', T) \rangle$  for S (green) and N' (purple). We also plot  $[\langle E_J(p', T) \rangle / k_B - T] = \rho_{sc}(p', T)$  for S (red) and N' (yellow). The smaller  $\rho_{sc}(p', T)$  of N' is the maximum critical current through the S-N'-S system [the superfluid density through S (red line) is larger] and is assumed to be proportional to the theoretical critical current  $J_c$  (dashed line).

The main reason to have supercurrents above  $T'_c = 25$  K is the presence of SC amplitudes  $\Delta_d$  in the CDW charge domains without LRO, what characterizes the PG region of the N' superconductor. Another important factor is the rearrangement of the holes between the layers according to subsequent experiments: using similar La-based materials but combining undoped insulators with overdoped metallic  $\text{La}_{2-x}\text{Sr}_x\text{CuO}_4$  with  $x = 0.38$ <sup>46</sup> and  $0.44$ <sup>47</sup>. The authors of those studies verified that the conducting holes pile up at the interface and redistribute themselves from the hole-rich to the insulator layers. Analysis with REXS<sup>46</sup> and  $\mu$ -SR<sup>47</sup> revealed that this reorganization of the holes occurs near the interface and they are not followed by the Sr dopant atoms. The rearrangement of the hole densities add on or subtract carriers and affect directly the local pair amplitudes  $\Delta_d$ , which depend on the local densities  $p(i)$  as discussed above. The redistribution and uniformization of the charges will enhance  $\langle \Delta_d \rangle$  in N' with a concomitant decrease in S.

This enhancement or weakening was observed in Meissner effects studies by low energy  $\mu$ -SR<sup>18</sup>. They showed that the local magnetic field  $\langle B_x \rangle$  along the  $z$  direction in a similar heterostructure S-N'-S is excluded like in a single uniform

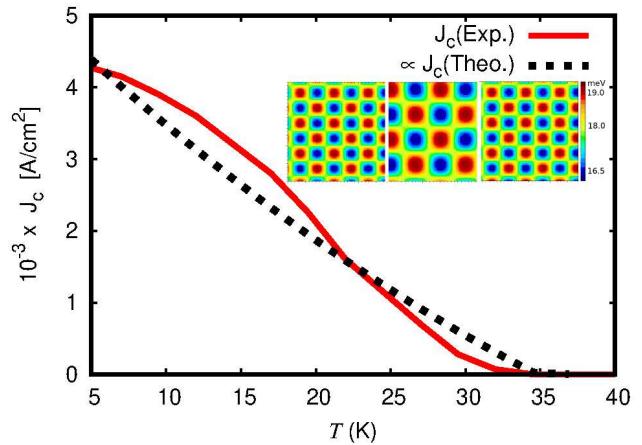


FIG. 5. The solid red line is the S-N'-S experimental results from Fig. 2 of Ref. [17], and the dashed line is our calculations that are proportional to  $J_c$ . We made both curves equal near  $T = 5$  K because our estimates are more precise at low temperatures. The inset shows schematically the coupled systems used in the calculations. In the trilayer experiments<sup>17,18</sup> the layers are on top of each other and connected by a small Josephson coupling, but in the text, we explain that the calculations are similar.

superconductor even at temperatures more than 3 times larger than  $T'_c$ . This reinforces our point that S and N' at  $T'_c < T < T_c$  have both the same structure differing only by the presence or absence of LRO in the charge domains.

Now we will apply these ideas to the GPE in the La-based trilayer system<sup>40</sup>. The effect of the checkerboard charge inhomogeneities in the local SC properties were studied in detail<sup>33</sup> in a system similar to N' with  $p = 0.12$ , and the simulations were shown above in Fig. 2. The  $\Delta_d(r_i)$  amplitude histogram is shown in Fig. 2(d), and the calculations show that CDW higher (lower) local hole densities have larger (smaller) local SC amplitudes<sup>9</sup>. Therefore, when a supercurrent flows, the S-N'-S system acquires a mean hole density close to their average; that is, the mean hole density in N' and S become  $p' \approx 0.135$ . This rearrangement increases  $\langle \Delta_d(N', T) \rangle$  by a factor of approximately 1.5 and decreases  $\langle \Delta_d(S, T) \rangle$  by a factor of approximately 0.6. Taking these changes into account, we calculate the new Josephson couplings in N' and S keeping their original  $R_n$  unchanged. The results of these calculations are shown in Fig. 4, where we plot these renormalized  $\langle E_J(p', T) \rangle$ , that is with  $p' = 0.135$  (green for S and purple for N') and  $\rho_{sc}(p', T)$  for the N' (yellow) and S (red) coupled layers. Since the critical current must be constant through the layers and N' holds the smaller values, we take exactly this (yellow) lower current as the theoretical critical current through the entire system (dashed line).

Since  $J_c = v_s \rho_{sc}$ ,  $v_s(p, T) \propto \langle E_J(p, T) \rangle / \langle E_J(p, 0) \rangle$ , and using the dashed  $\rho_{sc}(p', T)$  curve on Fig. 4, we obtain our estimation to the critical current measurements<sup>17</sup> shown in Fig. 5. To perform this comparison, we made our results equal to the lowest measured temperature  $T \approx 5$  K, where our estimation to  $v_s(T)$  is more precise. Our results follow near the experimental  $J_c(T)$  but do not have the round features dis-

played by the red curve that was taken from Ref. [17]. This is mainly because of the poor estimation of  $v_s(T)$  at finite temperatures. Another reason is that the S-N'-S system is formed with stacked layers along the  $z$  direction and our calculations are with layers in the CuO plane as shown in the inset of Fig. 5. But as discussed before, the calculations follow along the same lines in the sense that LRO is attained first in CuO planes and, afterward, by interlayer Josephson coupling, the whole system becomes superconducting. Another possible correction is that the  $z$ -direction current may enhance influences of out-of-plane dopants or oxygen interstitials<sup>30</sup>.

We argued that the formation of a granular superconductivity in the CO domains is the most basic property of cuprate superconductors. We showed that phase-ordering kinetics may describe electronic phase separation transitions by the GL potential  $V_{GL}$  with incommensurate free energy wells that originate the observed CDW. Charge fluctuations inside the domains may induce hole-hole SC interaction proportional to the depth of the  $V_{GL}$  wells averaging over the whole system, that is,  $\langle V_{GL}(p) \rangle$ <sup>9,15</sup>. The average Josephson coupling  $\langle E_J(p, T) \rangle$  between the local SC order parameter yields the LRO or phase-ordering temperature that is made equal to  $T_c$ . Furthermore,  $\langle E_J(p, T) \rangle - k_B T$  provides perfect agreement

with the measured superfluid density temperature dependence of La-based overdoped films<sup>40</sup>. The granular superconductivity is also the key mechanism behind the GPE because both S, N', and I (with nonzero doping) used in the experiments have all localized SC order parameters and differ only by the absence or presence of LRO.

We should emphasize that the Josephson coupling of Eq. 4 is inversely proportional to the resistivity, which leads to much smaller  $E_J$  inter-plane coupling, and its identification with the local superfluid density is confirmed by the anisotropic magnetic penetration length measurements<sup>37,38</sup>. We finish pointing out that the presence of CDW in electron-doped compounds<sup>48</sup> is a further indication that the method applies to all cuprates, and which we will explore further in the future.

## VI. ACKNOWLEDGEMENTS

We are grateful to David Möckli for critical reading the manuscript and acknowledge partial support by the Brazilian agencies CNPq and FAPERJ.

- 
- \* Corresponding author: evandro@mail.if.uff.br; Corresponding author: hercules\_santana@id.uff.br
- <sup>1</sup> B. Keimer, S. A. Kivelson, M. R. Norman, S. Uchida, and J. Zaanen, *Nature* **518**, 179–186 (2015).
  - <sup>2</sup> K. M. Lang, V. Madhavan, J. E. Hoffman, E. W. Hudson, H. Eisaki, S. Uchida, and J. C. Davis, *Nature* **415**, 412 (2002).
  - <sup>3</sup> R. Comin and A. Damascelli, *Ann. Rev. of Cond. Mat. Phys.* **7**, 369 (2016).
  - <sup>4</sup> J. W. Cahn and J. E. Hilliard, *J. Chem. Phys.* **28**, 258 (1958).
  - <sup>5</sup> E. V. L. de Mello, R. B. Kasal, and C. A. C. Passos, *J. Phys.: Condens. Matter* **21**, 235701 (2009).
  - <sup>6</sup> E. V. L. de Mello, *Europhys. Lett.* **99**, 37003 (2012).
  - <sup>7</sup> E. V. L. de Mello and R. B. Kasal, *Physica C: Superconductivity* **472**, 60 (2012).
  - <sup>8</sup> E. V. L. de Mello and J. E. Sonier, *J. Phys.: Condens. Matter* **26**, 492201 (2014).
  - <sup>9</sup> E. V. L. de Mello and J. E. Sonier, *Phys. Rev. B* **95**, 184520 (2017).
  - <sup>10</sup> J. Wu, A. T. Bollinger, X. He, and I. Božović, *Nature* **547**, 432 (2017).
  - <sup>11</sup> S.-D. Chen, M. Hashimoto, Y. He, D. Song, K.-J. Xu, J.-F. He, T. P. Devereaux, H. Eisaki, D.-H. Lu, J. Zaanen, and Z.-X. Shen, *Science* **366**, 1099 (2019).
  - <sup>12</sup> Y. Fei, Y. Zheng, K. Bu, W. Zhang, Y. Ding, X. Zhou, and Y. Yin, *Science China Physics, Mechanics & Astronomy* **63**, 227411 (2019).
  - <sup>13</sup> H. Miao, G. Fabbris, R. J. Koch, D. G. Mazzone, C. S. Nelson, R. Acevedo-Esteves, G. D. Gu, Y. Li, T. Yilimaz, K. Kaznatcheev, E. Vescovo, M. Oda, T. Kurosawa, N. Momono, T. Assefa, I.K. Robinson, E.S. Bozin, J.M. Tranquada, P.D. Johnson, M.P.M. Dean, *npj Quantum Materials* **6**, 31 (2021).
  - <sup>14</sup> B. I. Spivak and S. A. Kivelson, *Phys. Rev. B* **43**, 3740 (1991).
  - <sup>15</sup> E. V. L. de Mello, *J. of Phys.: Cond. Matter* **33**, 145503 (2021).
  - <sup>16</sup> R. S. Decca, H. D. Drew, E. Osquiguil, B. Maiorov, and J. Guimpel, *Phys. Rev. Lett.* **85**, 3708 (2000).
  - <sup>17</sup> I. Bozovic, G. Logvenov, M. A. J. Verhoeven, P. Caputo, E. Goldobin, and M. R. Beasley, *Phys. Rev. Lett.* **93**, 157002 (2004).
  - <sup>18</sup> E. Morenzoni, B. M. Wojek, A. Suter, T. Prokscha, G. Logvenov, and I. Bozovic, *Nature Communications* **2**, 272 (2011).
  - <sup>19</sup> E. de Mello and O. T. da Silveira Filho, *Physica A* **347**, 429 (2005).
  - <sup>20</sup> E. Fradkin, S. A. Kivelson, and J. M. Tranquada, *Rev. Mod. Phys.* **87**, 457 (2015).
  - <sup>21</sup> W. D. Wise, M. C. Boyer, K. Chatterjee, T. Kondo, T. Takeuchi, H. Ikuta, Y. Wang, and E. W. Hudson, *Nature Physics* **4**, 696 (2008).
  - <sup>22</sup> J. Chang, E. lackburn, T. Holmes, N. B. Christensen, J. Larsen, J. Mesot, R. Liang, D. A. Bonn, W. N. Hardy, A. Watenphul, M. V. Zimmermann, E. M. Forgan, and S. M. Hayden, *Nature Physics* **8**, 871 (2012).
  - <sup>23</sup> A. Bray, *Adv. Phys.* **43**, 357 (1994).
  - <sup>24</sup> J. M. Tranquada, B. J. Sternlieb, J. D. Axe, Y. Nakamura, and S. Uchida, *Nature* **375**, 561 (1995).
  - <sup>25</sup> V. Thampy, X. M. Chen, Y. Cao, C. Mazzoli, A. M. Barbour, W. Hu, H. Miao, G. Fabbris, R. D. Zhong, G. D. Gu, J. M. Tranquada, I. K. Robinson, S. B. Wilkins, and M. P. M. Dean, *Phys. Rev. B* **95**, 241111 (2017).
  - <sup>26</sup> Y. A. Kharkov and O. P. Sushkov, *Scientific Reports* **6**, 34551 (2016).
  - <sup>27</sup> “See supplemental material at [url will be inserted by publisher]for potential simulations and discussions.”
  - <sup>28</sup> R. Comin, R. Sutarto, E. H. da Silva Neto, L. Chauviere, R. Liang, W. N. Hardy, D. A. Bonn, F. He, G. A. Sawatzky, and A. Damascelli, *Science (New York, N.Y.)* **347**, 1335 (2015).
  - <sup>29</sup> H.-H. Kim *et al.*, *Phys. Rev. Lett.* **126**, 037002 (2021).
  - <sup>30</sup> G. Campi, A. Bianconi, N. Poccia, G. Bianconi, L. Barba, G. Arrighetti, D. Innocenti, J. Karpinski, N. D. Zhigadlo, S. M. Kazakov, M. Burghammer, M. v. Zimmermann, M. Sprung, and Ricci,

- Nature **525**, 359 (2015).
- <sup>31</sup> V. Ambegaokar and A. Baratoff, Phys. Rev. Lett. **10**, 486 (1963).
- <sup>32</sup> C. Bruder, A. van Otterlo, and G. T. Zimanyi, Phys. Rev. B **51**, 12904 (1995).
- <sup>33</sup> E. V. de Mello, J. Phys.: Condens. Matter **32**, 40LT02 (2020).
- <sup>34</sup> E. de Mello, J. Phys.: Condens. Matter **32**, 38LT01 (2020).
- <sup>35</sup> S. Ono and Y. Ando, Phys. Rev. B **67**, 104512 (2003).
- <sup>36</sup> S. Komiya, Y. Ando, X. F. Sun, and A. N. Lavrov, Phys. Rev. B **65**, 214535 (2002).
- <sup>37</sup> C. Panagopoulos, J. R. Cooper, T. Xiang, Y. S. Wang, and C. W. Chu, Phys. Rev. B **61**, R3808 (2000).
- <sup>38</sup> C. Panagopoulos, J. L. Tallon, and T. Xiang, Phys. Rev. B **59**, R6635 (1999).
- <sup>39</sup> V. J. Emery and S. A. Kivelson, Nature **374**, 434 (1995).
- <sup>40</sup> I. Božović, X. He, J. Wu, and A. T. Bollinger, Nature **536**, 309 (2016).
- <sup>41</sup> Y. J. Uemura, *et al.* Phys. Rev. Lett. **62**, 2317 (1989).
- <sup>42</sup> J. B. Ketterson and S. Song, *Superconductivity* (Cambridge University Press, London, 1999).
- <sup>43</sup> W. D. Wise, K. Chatterjee, M. C. Boyer, T. Kondo, T. Takeuchi, H. Ikuta, Z. Xu, J. Wen, G. D. Gu, Y. Wang, and E. W. Hudson, Nature Physics **5**, 213 (2009).
- <sup>44</sup> R. Comin, A. Frano, M. M. Yee, Y. Yoshida, H. Eisaki, E. Schierle, E. Weschke, R. Sutarto, F. He, A. Soumyanarayanan, He Yang, M. Le Tacon, I. S. Elfimov, E. Hoffman Jennifer, G. A. Sawatzky, B. Keimer, A. Damascelli, Science (New York, N.Y.) **343**, 390 (2014).
- <sup>45</sup> I. Bozovic, G. Logvenov, I. Belca, B. Narimbetov, and I. Sveklo, Phys. Rev. Lett. **89**, 107001 (2002).
- <sup>46</sup> S. Smadici, J. C. T. Lee, S. Wang, P. Abbamonte, G. Logvenov, A. Gozar, C. D. Cavellin, and I. Bozovic, Phys. Rev. Lett. **102**, 107004 (2009).
- <sup>47</sup> A. Suter, E. Morenzoni, T. Prokscha, H. Luetkens, B. Wojek, G. Logvenov, A. Gozar, and I. Božović, Physics Procedia **30**, 271 (2012).
- <sup>48</sup> E. H. da Silva Neto, M. Minola, B. Yu, W. Tabis, M. Bluschke, D. Unruh, H. Suzuki, Y. Li, G. Yu, D. Betto, K. Kummer, F. Yakhov, N. B. Brookes, M. Le Tacon, M. Greven, B. Keimer, A. Damascelli, Phys. Rev. B **98**, 161114 (2018).